BILINEAR MODELS FOR NONLINEAR UNMIXING OF HYPERSPECTRAL IMAGES

Yoann Altmann, Nicolas Dobigeon and Jean-Yves Tourneret

University of Toulouse, IRIT/INP-ENSEEIHT, France

{Yoann.Altmann, Nicolas.dobigeon, Jean-Yves.Tourneret}@enseeiht.fr

ABSTRACT

This paper compares several nonlinear models recently introduced for hyperspectral image unmixing. All these models consist of bilinear models that have shown interesting properties for hyperspectral images subjected to multipath effects. The first part of this paper presents different algorithms allowing the parameters of these models to be estimated. The relevance and flexibility of these models for spectral unmixing are then investigated by comparing the reconstruction errors and spectral angle mappers computed from synthetic and real dataset. This kind of study is important to determine which mixture model should be used in practical applications for hyperspectral image unmixing.

Index Terms— Hyperspectral imagery, unmixing, linear model, nonlinear model.

1. INTRODUCTION

Over the last few decades, spectral unmixing (SU) has been widely studied for hyperspectral image analysis. In SU, pixel spectra are usually assumed to be combinations of pure component spectra (endmembers) with a set of corresponding fractions (abundances) that indicate the proportion of each endmember present in a given pixel. The mixture model associated with spectral unmixing imagery can be linear or nonlinear, depending on the hyperspectral image under study. The linear mixing model (LMM) has shown interesting properties for macrospectral mixtures when the detected photons interact mainly with a single component on the scene before they reach the sensor. Mainly due to its ability to provide a simple first-order approximation, LMM is the most commonly encountered mixing model and has been widely studied in the literature. Conversely, nonlinear mixture models result from the interaction of photons with multiple components of the image. These nonlinear mixing models include models based on intimate mixtures [1] or bilinear models [2, 3, 4]. The first part of the paper reviews the bilinear models studied in the literature for nonlinear unmixing of remotely sensed hyperspectral images. These models are defined by spectral components appearing in the widely used LMM but also by bilinear terms corresponding to possible interactions between the different materials of the scene. The second part of the paper addresses the problem of supervised nonlinear SU of hyperspectral images by using bilinear models. Note that "supervised" means here that the endmembers contained in the image have been previously estimated by an endmember extraction algorithm (EEA). As a consequence, the parameters to be estimated are the mixing coefficients involved in the bilinear model under consideration and the noise variance. The paper is structured as follows. Section 2 recalls some elements of the widely used LMM (mainly to introduce notations). Section 3 presents the bilinear models that have been previously introduced in literature and that will be compared in this work. A comparison between the different bilinear models is conducted in Section 4 showing simulation results on synthetic and real images. Conclusions are finally reported in Section 5.

Part of this work has been funded by a grant from DGA (French Ministry of Defence).

2. LINEAR MIXING MODEL

The physical assumption underlying the LMM is that each incident photon interacts with one earth surface component only and that the reflected spectra do not mix before entering the sensor [5]. In that case, the L-spectrum $\mathbf{y} = [y_1, \ldots, y_L]^T$ of a mixed pixel can be expressed as a linear mixture of R endmembers $\mathbf{m}_r$ with additive noise

$$\mathbf{y} = \sum_{r=1}^{R} a_r \mathbf{m}_r + \mathbf{n} = \mathbf{M}\mathbf{a} + \mathbf{n}, \tag{1}$$

where $\mathbf{M}$ is an $L \times R$ matrix whose columns are the R endmember spectra $\mathbf{m}_r = [m_{1,r}, \ldots, m_{L,r}]^T$, $\mathbf{a} = [a_1, \ldots, a_R]^T$ is the fractional abundance vector and $\mathbf{n} = [n_1, \ldots, n_L]^T$ is an additive white noise sequence. The additive noise is classically assumed to be an independent and identically distributed (i.i.d) zero-mean Gaussian sequence with variance σ^2, denoted as $\mathbf{n} \sim \mathcal{N}\left(\mathbf{0}_L, \sigma^2 \mathbf{I}_L\right)$ where $\mathbf{I}_L$ is the identity matrix of dimension $L \times L$. As mentioned in the literature [5], the abundances must satisfy the following positivity and sum-to-one constraints

$$a_r \geq 0 \quad r = 1, \ldots, R, \quad \sum_{r=1}^{R} a_r = 1. \tag{2}$$

3. BILINEAR MODELS

Bilinear mixture models account for the presence of multiple photon interactions by introducing additional "interaction" terms in the LMM. This section presents bilinear mixing models previously introduced in the literature. These bilinear models mainly differ by the constraints associated with the mixing parameters.

3.1. Nascimento's bilinear mixing model

This section recalls the bilinear mixing model introduced in [2] referred to as "Nascimento's model" (NM) in this paper. The NM considers second order interactions between the ith and the jth endmembers (for $i, j = 1, \ldots R$ and $i \neq j$) such that the observed mixed pixel $\mathbf{y}$ can be written

$$\mathbf{y} = \sum_{r=1}^{R} a_r \mathbf{m}_r + \sum_{i=1}^{R-1} \sum_{j=i+1}^{R} \beta_{i,j} \mathbf{m}_i \odot \mathbf{m}_j + \mathbf{n} \tag{3}$$

where $\mathbf{m}_i \odot \mathbf{m}_j$ denotes the Hadamard (term-by-term) product of the ith and jth spectra:

$$\mathbf{m}_i \odot \mathbf{m}_j = \begin{pmatrix} m_{1,i} m_{1,j} \\ \vdots \\ m_{L,i} m_{L,j} \end{pmatrix}.$$

Note that the parameter $\beta_{i,j}$ in (3) is the amplitude of the interaction term due to the ith and jth components. According to [2], the unknown parameters $(\mathbf{a}, \beta_{1,2}, \ldots, \beta_{R-1,R})$ have to satisfy the following constraints

$$\begin{aligned} a_r \geq 0 \quad r = 1, \ldots, R, \\ \beta_{i,j} \geq 0 \quad i, j = 1, \ldots, R, \quad i \neq j \\ \sum_{r=1}^{R} a_r + \sum_{i=1}^{R-1} \sum_{j=i+1}^{R} \beta_{i,j} = 1. \end{aligned} \tag{4}$$

It is interesting to note that the NM can be seen as a linear mixture model with $R^* = \frac{1}{2}R(R+1)$ correlated endmembers. Indeed, by considering the interaction spectra $\mathbf{m}_i \odot \mathbf{m}_j$ as new spectral components with fractions $\beta_{i,j}$, model (3) can be rewritten

$$\mathbf{y} = \sum_{p=1}^{R^*} a_p^* \mathbf{m}_p^* + \mathbf{n} \tag{5}$$

where

$$\begin{aligned} a_p^* = a_r \quad , \quad \mathbf{m}_p^* = \mathbf{m}_r \quad p = 1, \ldots, R, \\ a_p^* = \beta_{i,j} \quad , \quad \mathbf{m}_p^* = \mathbf{m}_i \odot \mathbf{m}_j \quad R+1 \leq p \leq R^*. \end{aligned} \tag{6}$$

Consequently, the new abundance vector $\mathbf{a}^* = [a_1^*, \ldots, a_{R^*}^*]^T$ can be estimated using existing algorithms for linear SU, such as the FCLS algorithm [6] or the Bayesian algorithm introduced in [7]. Note also that the NM model reduces to the LMM when $a_p^* = 0$ for $p = R+1, \ldots, R^*$.

3.2. Fan's bilinear mixing model

This paragraph studies another bilinear mixing model introduced in [3] referred to as "Fan's model" (FM). Similarly to the NM, the FM assumes that the interaction terms $\mathbf{m}_i \odot \mathbf{m}_j$ are additional spectra, resulting from the Hadamard products of the pure spectral components. However, the FM assumes that the amplitudes of these interactions depends on the component fractions involved in the mixture. More precisely, according to the FM, an observed pixel of the hyperspectral image can be written

$$\mathbf{y} = \sum_{r=1}^{R} a_r \mathbf{m}_r + \sum_{i=1}^{R-1} \sum_{j=i+1}^{R} a_i a_j \mathbf{m}_i \odot \mathbf{m}_j + \mathbf{n}, \tag{7}$$

subject to the constraints (2). An unmixing procedure based on a Taylor series expansion and a least-squares method was proposed in [3] to estimate the unknown parameters involved in (7). Note however that other unmixing strategies such as the Bayesian algorithm introduced in [4] could be used for estimating the unknown FM parameters.

3.3. Generalized bilinear mixing model

This section presents a bilinear mixing model introduced in [4] for nonlinear SU and referred to as "generalized bilinear model" (GBM). As in the previous NM and FM, the interaction term $\mathbf{m}_i \odot \mathbf{m}_j$ is included in the GBM as an additional spectrum. However, the GBM assumes that the contribution of the interaction term $\mathbf{m}_i \odot \mathbf{m}_j$ is proportional to the fractions of the involved components with an amplitude $\gamma_{i,j} a_i a_j$ (it makes sense to assume that the "quantity" of interaction between two materials is related to the "quantity" of each material present in a given pixel), where $\gamma_{i,j} \in (0,1)$, leading to the following formulation

$$\mathbf{y} = \sum_{r=1}^{R} a_r \mathbf{m}_r + \sum_{i=1}^{R-1} \sum_{j=i+1}^{R} \gamma_{i,j} a_i a_j \mathbf{m}_i \odot \mathbf{m}_j + \mathbf{n}. \tag{8}$$

Note that $\boldsymbol{\gamma} = [\gamma_{1,2}, \ldots, \gamma_{R-1,R}]^T$ is a real parameter vector that quantifies the interactions terms between the different spectral components. The constraints associated with the GBM are expressed as

$$\begin{aligned} a_r \geq 0 \quad r = 1, \ldots, R, \quad \sum_{r=1}^{R} a_r = 1, \\ 1 \geq \gamma_{i,j} \geq 0 \quad i, j = 1, \ldots, R, \quad i \neq j. \end{aligned} \tag{9}$$

The main motivation for introducing the additional parameters $\gamma_{i,j}$ in the mixing model is to obtain a more flexible model than the NM or FM. Note that the GBM reduces to the LMM for $\gamma = \mathbf{0}$ (where $\mathbf{0}$ is an $(R^* - R) \times 1$ vector of zeros). Similarly, the GBM reduces to the FM for $\gamma = \mathbf{1}$, where $\mathbf{1}$ is an $(R^* - R) \times 1$ vector of ones. The unmixing procedure based on the GBM can be performed by using the Bayesian algorithm introduced in [4] or by using a least-squares estimator as in [3].

Remark: It is important to note that bilinear mixing models assume a deformation of the simplex spanned by the pixels resulting from the LMM. More precisely, the deformations related to the bilinear models presented above are shown in Fig. 1 for pixels defined by linear mixtures of $R = 3$ endmembers, where the data cloud composed of the observed pixels (blue points) is depicted in the space identified by a principal component analysis (PCA). Moreover, these results illustrate an interesting property: the pure spectra associated with the FM and the GBM are still endmembers, i.e., vertices of the clusters, contrary to the NM. In other words, endmember extraction algorithms based on geometrical interpretations, i.e., looking for the simplex of biggest [8, 9] or smallest volume [10, 11, 12], can still be used for both the FM and the GBM.

4. SIMULATIONS

4.1. Synthetic images

The accuracy of the linear (LMM) and non-linear (NM, FM and GBM) models is investigated by unmixing four synthetic images of 2500 pixels. The $R = 3$ endmembers associated with these images have been extracted from the spectral libraries provided with the ENVI software [13] (green grass, olive green paint and galvanized steel metal). The first synthetic image I_1 has been generated using the standard linear mixing model (LMM). The second and third images denoted as I_2 and I_3 have been generated according to the NM and FM respectively. Finally, the fourth image I_4 has been generated according to the GBM. In each case, 2500 abundance vectors $\mathbf{a}_n = (a_{n,1}, ..., a_{n,R})^T$ (for $n = 1, \ldots, 2500$) have been uniformly generated in the simplex defined by the positivity and sum-to-one

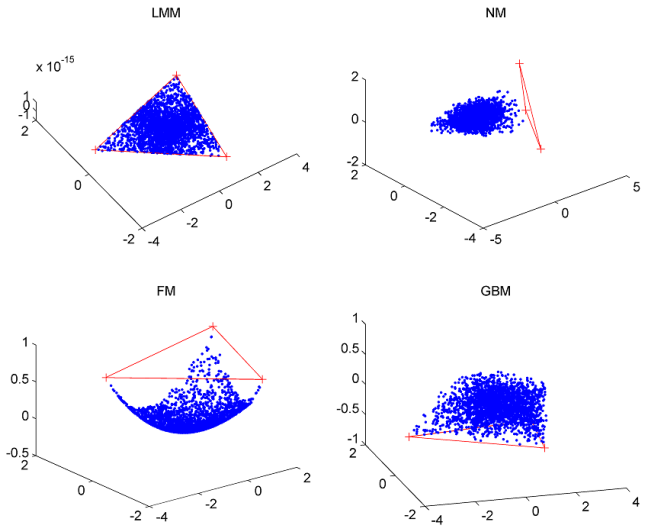

Fig. 1. Clusters of observations generated according to the LMM, the NM, the FM and the GBM (blue) and the corresponding endmembers (red).

constraints. To generate the fourth image I_4, the vectors $\boldsymbol{\gamma}_n$ (for $n = 1, \ldots, 2500$) of the GBM have been uniformly generated in the interval $[0, 1]$. All images have been corrupted by an additive Gaussian noise with signal-to-noise ratio $\text{SNR} = L^{-1}\sigma^{-2} \|f_{\text{M}}(\mathbf{a})\|^2 \simeq 15$dB, where $f_{\text{M}}(\mathbf{a})$ is defined from (3), (7) or (8) by removing the additive noise. The algorithms used to estimate the unknown model parameters are the FCLS for the LMM and NM, the dedicated algorithm of [3] for the FM and the Bayesian algorithm of [4] for the GBM. Note that we have observed that the different estimation algorithms provide similar performance for a given model (the only difference being in the execution time that can vary significantly from one algorithm to another).

The first criterion which is used to measure the quality of the unmixing algorithm is the reconstruction error

$$\text{RE} = \sqrt{\frac{1}{N}\sum_{n=1}^{N} \|\hat{\mathbf{y}}_n - \mathbf{y}_n\|^2}, \tag{10}$$

where $\mathbf{y}_n$ is the nth observation vector and $\hat{\mathbf{y}}_n$ its estimate. Table 1 shows the averaged REs obtained using the 4 mixing models and the 4 synthetic images of $P = 2500$ pixels. The quality of the different mixing models is then evaluated thanks to the spectral angle mapper (SAM) defined as the spectral distance between $\hat{\mathbf{y}}$ and $\mathbf{y}_n$

$$\text{SAM} = \arccos\left(\frac{\hat{\mathbf{y}}_n^T \mathbf{y}_n}{\|\hat{\mathbf{y}}_n\| \, \|\mathbf{y}_n\|}\right) \tag{11}$$

where arccos is the inverse cosine function. Table 2 compares the averaged SAMs for the four considered mixing models and the four synthetic images. These results shows that the GBM seems to be the more flexible model since it provides good unmixing performance for images generated according to the LMM, FM and GBM. However, the GBM seems to be less appropriate for images generated using the NM, probably because the NM endmembers are located much further from the simplex edges (see Fig. 1).

Table 1. Average REs on the synthetic images.

	RE (10^{-2})			
	I_1	I_2	I_3	I_4
LMM	**4.86**	9.17	6.02	5.32
NM	**4.86**	**4.40**	6.02	5.32
FM	5.93	10.90	5.25	5.55
GBM	4.87	9.24	**5.23**	**5.16**

Table 2. Average SAMs on the synthetic images.

	SAM (10^{-2})			
	I_1	I_2	I_3	I_4
LMM	**11.81**	15.17	12.61	12.16
NM	11.82	**9.56**	12.61	12.16
FM	13.79	25.06	11.64	12.52
GBM	11.82	15.14	**11.59**	**11.81**

4.2. Real data

The real image considered in this section is composed of $L = 203$ spectral bands (after removing the absorption water vapor bands) and was acquired in 1997 by the airborne visible infrared imaging spectrometer (AVIRIS) over Moffett Field (CA, USA). A sub-image of size 50×50 pixels has been chosen here to evaluate the proposed mixing models. The scene is mainly composed of water, vegetation and soil. The endmembers extracted by the VCA algorithm [9] (with $R = 3$) are displayed in Fig. 2. Fig. 3 shows the estimated abundance maps obtained by using the four previous mixing models and their corresponding estimation algorithms. The LMM, FM and GBM provide similar estimations for the Moffett scene. Note that the water abundance map estimated using the NM significantly differs from the water maps estimated assuming the LMM, FM and GBM. From the maps obtained with the FM and the GBM, the nonlinearities can be easily located mainly on the borders separating homogeneous areas. Fig. 4 shows the interaction terms obtained from the NM, FM and GBM. However, the water/vegetation interaction map estimated with NM shows high nonlinearities in the lake area, probably due to the low water reflectance. Since the water spectrum response is rather weak (Fig. 2, left), the interaction terms involving water are also of very low amplitude and the NM constraints are not strong enough to discriminate the close spectra water, water/vegetation and water/soil.

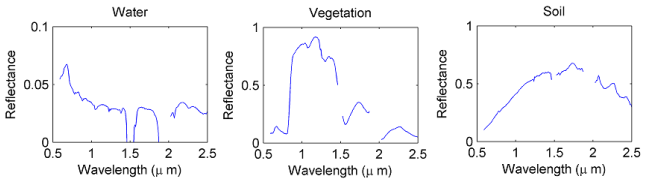

Fig. 2. The $R = 3$ endmembers estimated by the VCA on the Mofett scene.

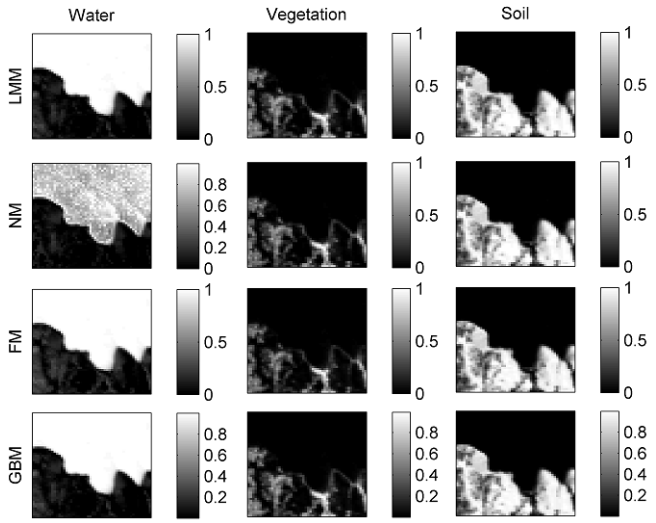

Fig. 3. Abundance maps estimated assuming LMM (1st row), NM (2st row), FM (3rd row) and GBM (4rd row).

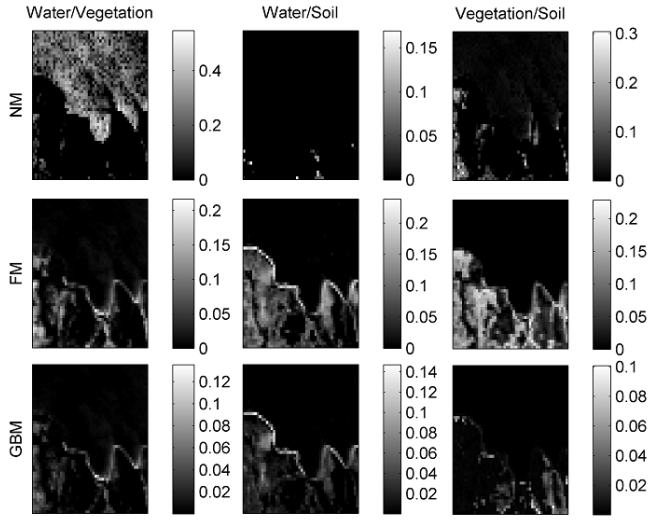

Fig. 4. Interaction maps estimated assuming NM (1st row), FM (2st row), and GBM (3rd row).

	RE (10^{-2})	SAM (10^{-2})
LMM	1.88	18.43
NM	1.83	17.17
FM	1.82	18.48
GBM	1.82	18.37

Table 3. Average REs and SAMs for the linear and bilinear models.

5. CONCLUSIONS

This paper studied several bilinear models for unmixing hyperspectral images. These models were previously introduced in the literature to take into account possible multipath effects occurring during the acquisition process. They were characterized by the inclusion of additional "virtual" endmember spectra coming from pairwise interactions of the endmembers actually present in the acquired scene. The main differences between these bilinear models are the constraints imposed on the interactions coefficients. Simulations on synthetic data were conducted to evaluate the accuracy and flexibility of these models, especially regarding model mismatch. Finally, experiments were conducted on a real hyperspectral image to illustrate the performance of the different mixing strategies.

6. REFERENCES

[1] B. W. Hapke, "Bidirectional reflectance spectroscopy. I. Theory," *J. Geophys. Res.*, vol. 86, pp. 3039–3054, 1981.

[2] J. M. P. Nascimento and J. M. Bioucas-Dias, "Nonlinear mixture model for hyperspectral unmixing," in *Proc. SPIE Image and Signal Processing for Remote Sensing XV*, L. Bruzzone, C. Notarnicola, and F. Posa, Eds., vol. 7477. Berlin, Germany: SPIE, Sept. 2009, pp. 74 770I–1–74 770I–8.

[3] W. Fan, B. Hu, J. Miller, and M. Li, "Comparative study between a new nonlinear model and common linear model for analysing laboratory simulated-forest hyperspectral data," *Remote Sensing of Environment*, vol. 30, no. 11, pp. 2951–2962, June 2009.

[4] A. Halimi, Y. Altmann, N. Dobigeon, and J.-Y. Tourneret, "Nonlinear unmixing of hyperspectral images using a generalized bilinear model," *IEEE Trans. Geosci. and Remote Sensing*, 2011, to appear.

[5] N. Keshava and J. F. Mustard, "Spectral unmixing," *IEEE Signal Processing Magazine*, pp. 44–57, Jan. 2002.

[6] D. C. Heinz and C.-I Chang, "Fully constrained least-squares linear spectral mixture analysis method for material quantification in hyperspectral imagery," *IEEE Trans. Geosci. and Remote Sensing*, vol. 29, no. 3, pp. 529–545, March 2001.

[7] N. Dobigeon, J.-Y. Tourneret, and C.-I Chang, "Semi-supervised linear spectral unmixing using a hierarchical Bayesian model for hyperspectral imagery," *IEEE Trans. Signal Process.*, vol. 56, no. 7, pp. 2684–2695, July 2008.

[8] M. Winter, "Fast autonomous spectral end-member determination in hyperspectral data," in *Proc. 13th Int. Conf. on Applied Geologic Remote Sensing*, vol. 2, Vancouver, April 1999, pp. 337–344.

[9] J. M. Nascimento and J. M. Bioucas-Dias, "Vertex component analysis: A fast algorithm to unmix hyperspectral data," *IEEE Trans. Geosci. and Remote Sensing*, vol. 43, no. 4, pp. 898–910, April 2005.

[10] M. Craig, "Minimum volume transforms for remotely sensed data," *IEEE Trans. Geosci. and Remote Sensing*, pp. 542–552, 1994.

[11] L. Miao and H. Qi, "Endmember extraction from highly mixed data using minimum volume constrained nonnegative matrix factorization," *IEEE Trans. Geosci. and Remote Sensing*, vol. 45, no. 3, pp. 765–777, March 2007.

[12] J. Li and J. M. Bioucas-Dias, "Minimum volume simplex analysis: a fast algorithm to unmix hyperspectral data," in *Proc. IEEE Int. Conf. Geosci. and Remote Sensing (IGARSS)*, vol. 3, Boston, USA, July 2008, pp. 250–253.

[13] RSI (Research Systems Inc.), *ENVI User's guide Version 4.0*, Boulder, CO 80301 USA, Sept. 2003.